

Neural Network-Based Nonlinear Dynamic Inversion Control of Variable-Span Morphing Aircraft

Jihoon Lee* and Youdan Kim*[†]

*Seoul National University

Seoul 08826, Republic of Korea

leejihoon@snu.ac.kr · ydkim@snu.ac.kr

[†]Corresponding author

Abstract

Morphing aircraft is an aircraft that can change its configuration during the flight. Aircraft morphing technology is one of the methods that may improve the performance of the aircraft for various flight conditions. In this study, nonlinear control augmentation system for the morphing aircraft is proposed using nonlinear dynamic inversion based on neural network. Two-layer feed-forward neural networks are used to obtain longitudinal and lateral inverse maps which convert desired aerodynamic moments into actual control commands. Numerical simulation is performed for two maneuvers to demonstrate the effectiveness of the proposed scheme.

Nomenclature

\bar{q}	Dynamic pressure
$\delta a, \delta e, \delta r$	Aileron, elevator and rudder deflections
η	Morphing parameter
ϕ, θ, ψ	Roll, pitch and yaw angles defined by 3-2-1 Euler rotation sequence
a_n, a_y	Normal and lateral accelerations in g's
C_l, C_m, C_n	Rolling, pitching and yawing moment coefficients
g	Gravitational acceleration
g_0	Scaling factor used for conversion of acceleration into g's
J	Body-axis moment of inertia matrix
K_1, K_2, K_3, K_4	Proportional and integral gains for normal and lateral acceleration control
$K_{p_\phi}, K_{d_\phi}, K_{p_\theta}, K_{d_\theta}, K_{p_\psi}, K_{d_\psi}$	Roll, pitch and yaw-axis proportional and derivative gains
l, m, n	Rolling, pitching and yawing moments
P, Q, R	Roll, pitch and yaw rates
S, b, \bar{c}	Wing planform area, wingspan and mean aerodynamic chord
U, V, W	Body x, y and z-axis components of aircraft velocity
u_ϕ, u_θ, u_ψ	Pseudo-control variables for roll, pitch and yaw angle control
u_n, u_y	Pseudo-control variables for normal and lateral acceleration control
V_T, α, β	Airspeed, angle of attack and sideslip angle

1. Introduction

Development of aircraft morphing technology has a long history, which starts from the beginning of aircraft.¹ Since the introduction of the morphing concept, research efforts regarding aircraft morphing technology have been focused on the fields of materials, structural and aerodynamic sciences. Aircraft capable of changing their external shape during the flight have many advantages compared to conventional fixed-shape aircraft which can be controlled only by hinged aerodynamic control surfaces. In the design process of conventional aircraft, there exist inherent compromises between the performance which may be significantly relieved by exploiting morphing technology and adapting wing configuration in accordance with flight conditions and missions. However, configuration change during the flight may cause undesirable effects including unsteady aerodynamic effects, time-varying moment of inertia and variations in the location of the center of gravity, which make the design of morphing aircraft flight control systems complicated. Consequently, to take full advantage of morphing and maximize the performance while ensuring stability, control designers should incorporate all these effects to control systems.

To deal with configuration change of the morphing aircraft, various control schemes have been applied, e.g. switched H_∞ control,² linear parameter-varying (LPV) control^{3,4} and adaptive control.^{5,6} There exist also various research on morphing aircraft control design.⁷⁻¹² Variations in morphing aircraft's static and dynamic characteristics during transition process have been analyzed.^{13,14} Morphing may change the vehicle's performance, and generate control forces and moments. Roll control can be achieved by twist morphing,¹⁵ and variable cant angle winglet can be used to control both longitudinal and lateral directions.¹⁶

Morphing aircraft have been modeled as a multi-body dynamic model,¹⁷ LPV system¹⁸ and linear time-varying (LTV) system.¹⁹ Determination of optimal morphing configuration in terms of aerodynamics has been also studied by aerodynamic designers. Although morphing actuator dynamics is often neglected in the design process of flight control system, morphing control itself is also an essential part of morphing aircraft flight control system. Furthermore, analysis on dynamic loading^{20,21} can be critical for out-of-plane morphing, and it is closely related to the control allocation problem.

Neural network-based adaptive control,²²⁻²⁴ neural network-based dynamic inversion control²⁵⁻²⁷ and neural network-based adaptive dynamic inversion control^{28,29} have been successfully applied to conventional aircraft. In this study, command augmentation system (CAS), whose structure was proposed by Menon,³⁰ is generalized for the implementation on morphing aircraft control system. CAS for morphing aircraft should incorporate variations in moment of inertia matrix and aerodynamic coefficients which are utilized in nonlinear dynamic inversion based on neural network. Two-layer (hidden layer and output layer) neural networks are designed and trained to map desired aerodynamic coefficients, which are intermediate outputs in the model inversion process, into control surface deflection commands. Strength of the feed-forward neural network lies in its low computational burden which must be ensured for real-time control. Mean squared errors for each combination of backpropagation algorithms and hidden layer structures are evaluated, and the best combination in terms of performance and overfitting is used for the CAS. Numerical simulation is performed for two challenging maneuvers to demonstrate the effectiveness of the proposed scheme in controlling variable-span morphing aircraft. A high performance aircraft model is adopted as a nominal non-morphing aircraft model and the effects of morphing are modeled as functions of the morphing parameter. Simulation results show that morphing aircraft can be controlled effectively and efficiently by the proposed scheme.

2. Morphing Aircraft Model

An F-18 high-alpha research vehicle (HARV) model is adopted as a baseline model and modified to emulate the effects of span morphing. As shown in Fig. 1, it is assumed that there are moving parts at both ends of the main wing whose mean aerodynamic chord (mac) is \bar{c}_m , and maximum span-wise extra length is b_η . The morphing parameter η is defined as a ratio of the extended length to the maximum extra length. An F-18 HARV has five aerodynamic control surfaces: a pair of ailerons, a pair of differential stabilators and a rudder. In this study, left and right stabilators are assumed to be synchronized and treated as an elevator throughout the modeling and simulation. Moment coefficients of the morphing aircraft model can be represented as follows

$$\begin{aligned}
 C_l(V_T, \alpha, \beta, P, R, \delta a, \delta r, \eta) &= \left[C_{l_\beta}(\alpha)\beta + \frac{b}{2V_T}C_{l_p}(\alpha)P + \frac{b}{2V_T}C_{l_R}(\alpha)R \right] \Lambda_{lat}(\eta) + C_{l_{\delta a}}(\alpha)\delta a + C_{l_{\delta r}}(\alpha)\delta r \\
 C_m(V_T, \alpha, Q, \delta e, \eta) &= \left[C_{m_0}(\alpha) + \frac{\bar{c}}{2V_T}C_{m_Q}(\alpha)Q \right] \Lambda_{lon}(\eta) + C_{m_{\delta e}}(\alpha)\delta e \\
 C_n(V_T, \alpha, \beta, P, R, \delta a, \delta r, \eta) &= \left[C_{n_\beta}(\alpha)\beta + \frac{b}{2V_T}C_{n_p}(\alpha)P + \frac{b}{2V_T}C_{n_R}(\alpha)R \right] \Lambda_{lat}(\eta) + C_{n_{\delta a}}(\alpha)\delta a + C_{n_{\delta r}}(\alpha)\delta r
 \end{aligned} \tag{1}$$

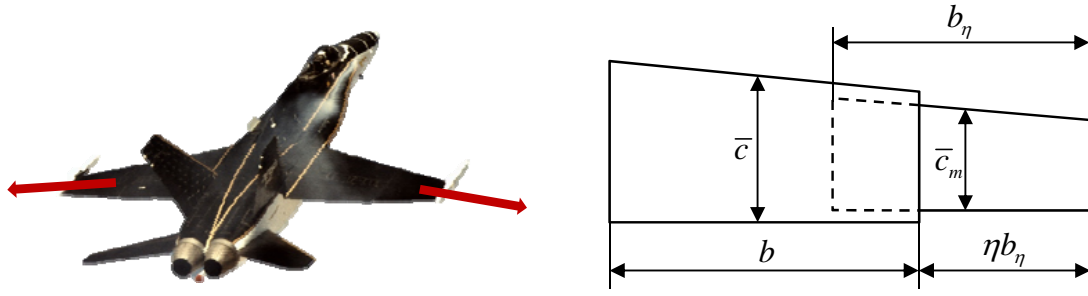


Figure 1: Definition of morphing parameter

where the effects of span variation on the coefficients are modeled by following two functions Λ_{lon} and Λ_{lat} , which depend on morphing parameter η .

$$\begin{aligned}\Lambda_{lon}(\eta) &= \Lambda_S(\eta)\Lambda_{\bar{c}}(\eta) \\ \Lambda_{lat}(\eta) &= \Lambda_S(\eta)\Lambda_b(\eta)\end{aligned}\quad (2)$$

where

$$\begin{aligned}\Lambda_S(\eta) &= 1 + \frac{\bar{c}_m b_\eta}{S} \eta \\ \Lambda_b(\eta) &= 1 + \frac{b_\eta}{b} \eta \\ \Lambda_{\bar{c}}(\eta) &= \frac{1 + \frac{\bar{c}_m}{\bar{c}} \frac{b_\eta}{b} \eta}{1 + \frac{b_\eta}{b} \eta}\end{aligned}\quad (3)$$

Similarly, lift, drag and side force (wind-axis) coefficients can be represented as follows.

$$\begin{aligned}C_L(V_T, \alpha, Q, \delta e, \eta) &= \left[C_{L_0}(\alpha) + \frac{\bar{c}}{2V_T} C_{L_Q}(\alpha) Q \right] \Lambda_S(\eta) + C_{L_{\delta e}}(\alpha) \delta e \\ C_D(V_T, \alpha, Q, \delta e, \eta) &= \left[C_{D_0}(\alpha) + \frac{\bar{c}}{2V_T} C_{D_Q}(\alpha) Q \right] \Lambda_S(\eta) + C_{D_{\delta e}}(\alpha) \delta e \\ C_{Y_w}(V_T, \alpha, \beta, P, R, \delta a, \delta r, \eta) &= \left[C_{Y_{w\beta}}(\alpha) \beta + \frac{b}{2V_T} C_{Y_{wP}}(\alpha) P + \frac{b}{2V_T} C_{Y_{wR}}(\alpha) R \right] \Lambda_S(\eta) + C_{Y_{w\delta a}}(\alpha) \delta a + C_{Y_{w\delta r}}(\alpha) \delta r\end{aligned}\quad (4)$$

The above Λ functions are introduced by mimicking variations in the reference area and lengths considering that general behaviors of aerodynamic coefficients and their dependency on α would be approximately the same, only scaling up and down in response to extra span. Note that emphasis is on generalization and application of the existing framework to an aircraft that can change its shape during the flight rather than high-fidelity modeling of morphing itself. Moving parts are assumed to move along body y-axis only. Consequently, J_{yy} and J_{xz} remain unchanged regardless of span variations. By applying the parallel axis theorem, x and z-axis components of the moment of inertia matrix is represented as follows

$$\begin{aligned}J_{xx} &= J_{xx_0} - m_m \left(b - \frac{1}{2} b_\eta \right)^2 + m_m \left(b - \frac{1}{2} b_\eta + \eta b_\eta \right)^2 \\ J_{zz} &= J_{zz_0} - m_m \left(b - \frac{1}{2} b_\eta \right)^2 + m_m \left(b - \frac{1}{2} b_\eta + \eta b_\eta \right)^2\end{aligned}\quad (5)$$

where m_m is the mass of the moving parts.

3. Command Augmentation System

In this section, nonlinear CAS is briefly explained, whose structure is adopted from Menon.³⁰ CAS receives pilot commands of roll rate and normal acceleration, and generates actual control surface deflection commands required to accomplish the commands. Proportional-integral and proportional-derivative control laws are used in the nonlinear dynamic inversion. The later part of the CAS is composed of dynamic and aerodynamic model inversion based on neural network.

3.1 Command Augmentation Logic

In the command augmentation logic, the normal acceleration command is assumed to be given from a pilot and the lateral acceleration command is always set to zero for turn coordination. Derivation of the logic starts from the flat-earth (NED) body-axis translational equations of motion.

$$\begin{aligned}\dot{V} &= -RU + PW - g \sin \phi \cos \theta + a_y g_0 \\ \dot{W} &= QU - PV - g \cos \phi \cos \theta + a_z g_0\end{aligned}\quad (6)$$

Following proportional-integral control laws for acceleration control are used.

$$\begin{aligned}u_n &= K_1(a_{nc} - a_n) + K_2 \int (a_{nc} - a_n) dt \\ u_y &= K_3(a_{yc} - a_y) + K_4 \int (a_{yc} - a_y) dt\end{aligned}\quad (7)$$

The pitch and yaw rate commands to follow the acceleration commands can be expressed as follows.

$$\begin{aligned}Q_c &= K_1 \frac{1}{U} g_0 (a_{nc} - a_n) + K_2 \frac{1}{U} \int g_0 (a_{nc} - a_n) dt + \frac{1}{U} (PV + g \cos \phi \cos \theta) \\ R_c &= K_3 \frac{1}{U} g_0 (a_{yc} - a_y) + K_4 \frac{1}{U} \int g_0 (a_{yc} - a_y) dt + \frac{1}{U} (PW + g \sin \phi \cos \theta)\end{aligned}\quad (8)$$

It is assumed that \dot{V} and \dot{W} are negligible. This assumption can be justified due to the fact that translational dynamics of fixed-wing aircraft is significantly slower than its rotational dynamics. Pitch and yaw rate commands generated in the command augmentation logic are used in the attitude control system.

3.2 Attitude Control System

Through the Euler angle kinematic differential equations, Euler angle rate commands can be expressed as follows

$$\begin{bmatrix} \dot{\phi}_c & \dot{\theta}_c & \dot{\psi}_c \end{bmatrix}^T = H(\Omega) \begin{bmatrix} P_c & Q_c & R_c \end{bmatrix}^T \quad (9)$$

where $\Omega = \begin{bmatrix} \phi & \theta & \psi \end{bmatrix}^T$, and $H(\Omega)$ is defined as follows.

$$H(\Omega) = \begin{bmatrix} 1 & \sin \phi \tan \theta & \cos \phi \tan \theta \\ 0 & \cos \phi & -\sin \phi \\ 0 & \sin \phi \sec \theta & \cos \phi \sec \theta \end{bmatrix} \quad (10)$$

By taking derivative of the kinematic differential equations, the following second-order differential equations can be obtained.

$$\begin{bmatrix} \ddot{\phi} \\ \ddot{\theta} \\ \ddot{\psi} \end{bmatrix} = \dot{\phi} \begin{bmatrix} 0 & \cos \phi \tan \theta & -\sin \phi \tan \theta \\ 0 & -\sin \phi & -\cos \phi \\ 0 & \cos \phi \sec \theta & -\sin \phi \sec \theta \end{bmatrix} \begin{bmatrix} P_c \\ Q_c \\ R_c \end{bmatrix} + \dot{\theta} \begin{bmatrix} 0 & \sin \phi \sec^2 \theta & \cos \phi \sec^2 \theta \\ 0 & 0 & 0 \\ 0 & \sin \phi \sec \theta \tan \theta & \cos \phi \sec \theta \tan \theta \end{bmatrix} \begin{bmatrix} P_c \\ Q_c \\ R_c \end{bmatrix} + H(\Omega) \begin{bmatrix} \dot{P} \\ \dot{Q} \\ \dot{R} \end{bmatrix} \quad (11)$$

Proportional-derivative control laws of the following form are used for Euler angle control.

$$\begin{aligned}u_\phi &= K_{p_\phi}(\phi_c - \phi) + K_{d_\phi}(\dot{\phi}_c - \dot{\phi}) \\ u_\theta &= K_{p_\theta}(\theta_c - \theta) + K_{d_\theta}(\dot{\theta}_c - \dot{\theta}) \\ u_\psi &= K_{p_\psi}(\psi_c - \psi) + K_{d_\psi}(\dot{\psi}_c - \dot{\psi})\end{aligned}\quad (12)$$

The above attitude controller makes Euler angles have globally asymptotically stable linear second-order dynamics if \dot{P} , \dot{Q} and \dot{R} that exactly corresponds to the commanded pseudo-control variables u_ϕ , u_θ and u_ψ can be generated. The remaining work is to recover actual control surface deflections generating the desired body rate derivatives, which will be covered in the following section.

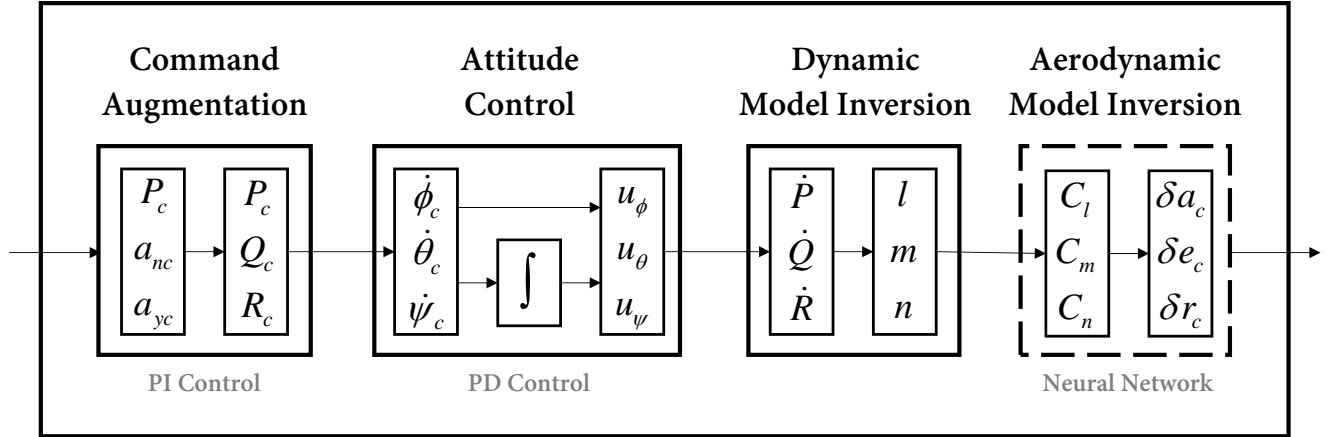


Figure 2: Command augmentation system for morphing aircraft

4. Model Inversion

Control surface deflection commands can be recovered from the desired angular velocity rates through a procedure called model inversion. Inversion process is divided into two steps. The first step of model inversion exploits the knowledge of kinematic relations and rotational dynamics. This is done through exact calculations where even quasi-statically-varying moment of inertia can be treated. The second step requires computation using detailed knowledge of aerodynamic and control derivatives which can be replaced by function-fitting neural network. Exact inversion usually requires a lot of interpolation operations which may cause excessive computational burdens depending on the constructed model. In contrast, feed-forward neural network-based inversion requires only simple operations such as addition, multiplication and activation function evaluation. In addition, neural network has potential of relieving predefined structure of aerodynamic coefficients' component such as linear dependency of control surface deflections, which may enable precise inversion for a highly nonlinear model.

4.1 Dynamic Model Inversion

Pre-multiplying Eq. (9) by $H^{-1}(\Omega)$ and taking derivatives yield the following expression for the desired angular velocity rates.

$$\begin{bmatrix} \dot{P} \\ \dot{Q} \\ \dot{R} \end{bmatrix} = \dot{\phi} \begin{bmatrix} 0 & 0 & 0 \\ 0 & -\sin \phi & \cos \phi \cos \theta \\ 0 & -\cos \phi & -\sin \phi \cos \theta \end{bmatrix} \begin{bmatrix} \dot{\phi} \\ \dot{\theta} \\ \dot{\psi} \end{bmatrix} + \dot{\theta} \begin{bmatrix} 0 & 0 & -\cos \theta \\ 0 & 0 & -\sin \phi \sin \theta \\ 0 & 0 & -\sin \phi \sin \theta \end{bmatrix} \begin{bmatrix} \dot{\phi} \\ \dot{\theta} \\ \dot{\psi} \end{bmatrix} + \begin{bmatrix} 1 & 0 & -\sin \theta \\ 0 & \cos \phi & \sin \phi \cos \theta \\ 0 & -\sin \phi & \cos \phi \cos \theta \end{bmatrix} \begin{bmatrix} u_\phi \\ u_\theta \\ u_\psi \end{bmatrix} \quad (13)$$

The moments required to achieve the desired body rates can be recovered from the body-axis rotational equations of motion of the following form.

$$\begin{bmatrix} l \\ m \\ n \end{bmatrix} = J \begin{bmatrix} \dot{P} \\ \dot{Q} \\ \dot{R} \end{bmatrix} + \begin{bmatrix} 0 & -R & Q \\ R & 0 & -P \\ -Q & P & 0 \end{bmatrix} J \begin{bmatrix} P \\ Q \\ R \end{bmatrix} \quad (14)$$

Note that this process enables the CAS to exactly compensate for the effects of possible variations in moment of inertia. In practice, this is an integral part of the CAS in order to be implementable on the control system of the morphing aircraft where the moment of inertia may vary in large scale. From the definitions of the aerodynamic coefficients, the values of the aerodynamic coefficients corresponding to the moments are expressed as follows.

$$C_l = \frac{l}{\bar{q}Sb}, \quad C_m = \frac{m}{\bar{q}S\bar{c}}, \quad C_n = \frac{n}{\bar{q}Sb},$$

The above aerodynamic coefficients will be put into the neural networks together with flight state variables.

4.2 Exact Aerodynamic Model Inversion

Equation (1) can be rewritten in a more concise form as follows

$$\begin{bmatrix} C_l \\ C_m \\ C_n \end{bmatrix} = \begin{bmatrix} f_1 \\ f_2 \\ f_3 \end{bmatrix} + \begin{bmatrix} g_1 & g_2 & g_3 \\ g_4 & g_5 & g_6 \\ g_7 & g_8 & g_9 \end{bmatrix} \begin{bmatrix} \delta a \\ \delta e \\ \delta r \end{bmatrix} \quad (15)$$

where f_i and g_j are functions of state variables and the morphing parameter. The inverse relation from aerodynamic coefficients to control surface deflections can be written as follows.

$$\begin{bmatrix} \delta a \\ \delta e \\ \delta r \end{bmatrix} = \begin{bmatrix} g_1 & g_2 & g_3 \\ g_4 & g_5 & g_6 \\ g_7 & g_8 & g_9 \end{bmatrix}^{-1} \begin{bmatrix} C_l - f_1 \\ C_m - f_2 \\ C_n - f_3 \end{bmatrix} \quad (16)$$

Now the complete structure of the CAS can be constructed as illustrated in Fig. 2. The CAS consists of command augmentation logic, attitude control system and nonlinear model inversion using neural network. The inversion shown in Eq. (16) can be achieved by exploiting complete information of the aerodynamic and control derivatives. Although exact inversion guarantees the most desirable performance, it is computationally expensive to be performed on-board especially when a high-fidelity model is used. Therefore, the results of the exact inversion will be used only as a reference for evaluation of the performance of neural network-based inversion.

4.3 Approximate Aerodynamic Model Inversion Using Neural Network

Input-output pairs of control surface deflections and the resulting aerodynamic coefficients can be generated through either a high-fidelity model or actual flight tests under the assumption that all state variables are known. In this study, 4,096 data for a longitudinal neural network and 65,536 data for a lateral neural network were generated using an F-18 HARV model. Combinations of control surface deflections and state variables were generated randomly and uniformly throughout the flight region given in Tables 1 and 2. The generated data are normalized so that all inputs and targets have values from 0 to 1 and then randomly divided into 70% samples for training, 15% samples for test and 15% samples for validation. The samples are used to train two two-layer feed-forward neural networks: a longitudinal channel neural network whose output is δe , and a lateral channel neural network whose outputs are δa and δr . Each neural network is trained using various combinations of hidden layer sizes and backpropagation algorithms.

Table 1: Training region for longitudinal neural network

	δe	α	M	h	Q	η	C_m^*
Lower bound	-24°	-2°	0.4	0m	-1.5 rad/s	0	-0.49
Upper bound	10.5°	12°	1.2	10,000m	1.5 rad/s	1	0.71

*Generated from set of other variables

Table 2: Training region for lateral neural network

	δa	δr	α	M	h	P	R	η	C_l^*	C_n^*
Lower bound	-35°	-30°	-2°	0.4	0m	-1.5 rad/s	-1 rad/s	0	-0.11	-0.06
Upper bound	35°	30°	12°	1.2	10,000m	1.5 rad/s	1 rad/s	1	0.11	0.06

*Generated from set of other variables

4.4 Training Results

Neural networks with various hidden layer sizes from 5 to 50 were trained using four different back-propagation algorithms. Mean squared error (MSE) is a typical measure of performance of a neural network, and the sum of absolute values of the weights is one of the most widely used measures of how much the neural network is overfitting the data. The two measures corresponding to each neural network are shown in Figs. 3 and 4. As the hidden layer size increases, the MSE tends to decrease and the sum of the weights tends to increase, which clearly shows that there is a trade-off relation between the performance (MSE) and overfitting (weight sum). By investigating the training results shown in Figs. 3 and 4, the size of hidden layer is chosen to be 15 for the longitudinal network and 25 for the lateral network, and the Bayesian regularization backpropagation algorithm is used for both networks.

NEURAL NETWORK-BASED NONLINEAR DYNAMIC INVERSION CONTROL OF VARIABLE-SPAN MORPHING AIRCRAFT

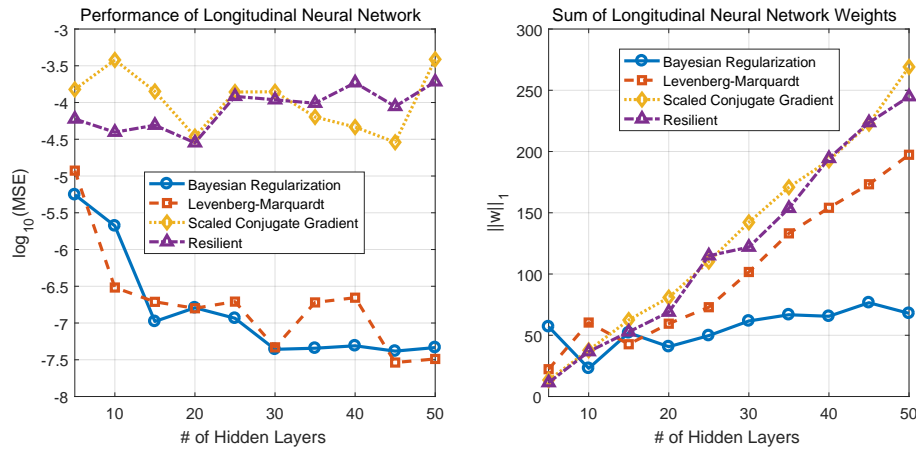


Figure 3: Longitudinal channel training results

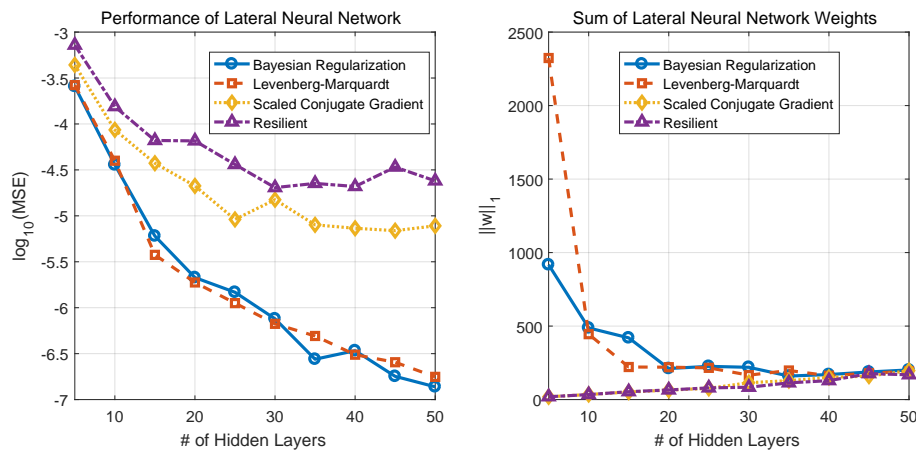


Figure 4: Lateral channel training results

5. Numerical Simulation

In this section, numerical simulation results are presented. Two maneuvers are examined: i) push-over and pull-up, and ii) high-g turn. Prescribed morphing parameter scenarios is applied to assist the maneuver where pilot commands are identical to those in Kim³¹ and Kim and Calise.³² Figures 5 and 6 show the results of the push-over and pull-up scenario where exact inversion and neural network-based inversion are used. Figure 7 and 8 show the results of the high-g turn scenario where exact inversion and neural network-based inversion are used. Throttle is set to 0.4 and 1.0 throughout the maneuvers in each scenario. In all the scenarios, initial altitude was set to 2,500m and initial Mach number was set to 0.6.

The most obvious difference between the results of exact and neural network-based inversion can be found in Figs. 5 and 6. While exact inversion does not cause any perturbations along the lateral direction, neural network-based inversion induces a little use of both an aileron and a rudder. Even though this difference is apparently attributed to the inversion error, deviations in roll and pitch angles and roll and pitch rates from zero are less than 0.01° and $0.01^\circ/\text{s}$. These errors are not significant so that it is barely noticeable in Figs. 7 and 8. In addition, the differences of altitude loss for the entire 30 seconds in both scenarios are smaller than 1m out of a few thousands meters total altitude loss.

In the first scenario, a morphing wingspan is constantly increased until the first 15 seconds to prevent drastic loss in altitude and then maintains a fully-deployed state for the remaining 15 seconds to help the vehicle achieve the commanded 4g normal acceleration by widening the overall lifting surface area. On the other hand, in the second scenario, a morphing wingspan is constantly retracted during the first 8 seconds to obtain enough roll-axis maneuverability to follow the $10^\circ/\text{s}$ roll rate command. Once the vehicle achieves roll angle of 80° , a morphing command is given to increase the wingspan again up to the maximum length throughout the remaining time.

NEURAL NETWORK-BASED NONLINEAR DYNAMIC INVERSION CONTROL OF VARIABLE-SPAN MORPHING AIRCRAFT

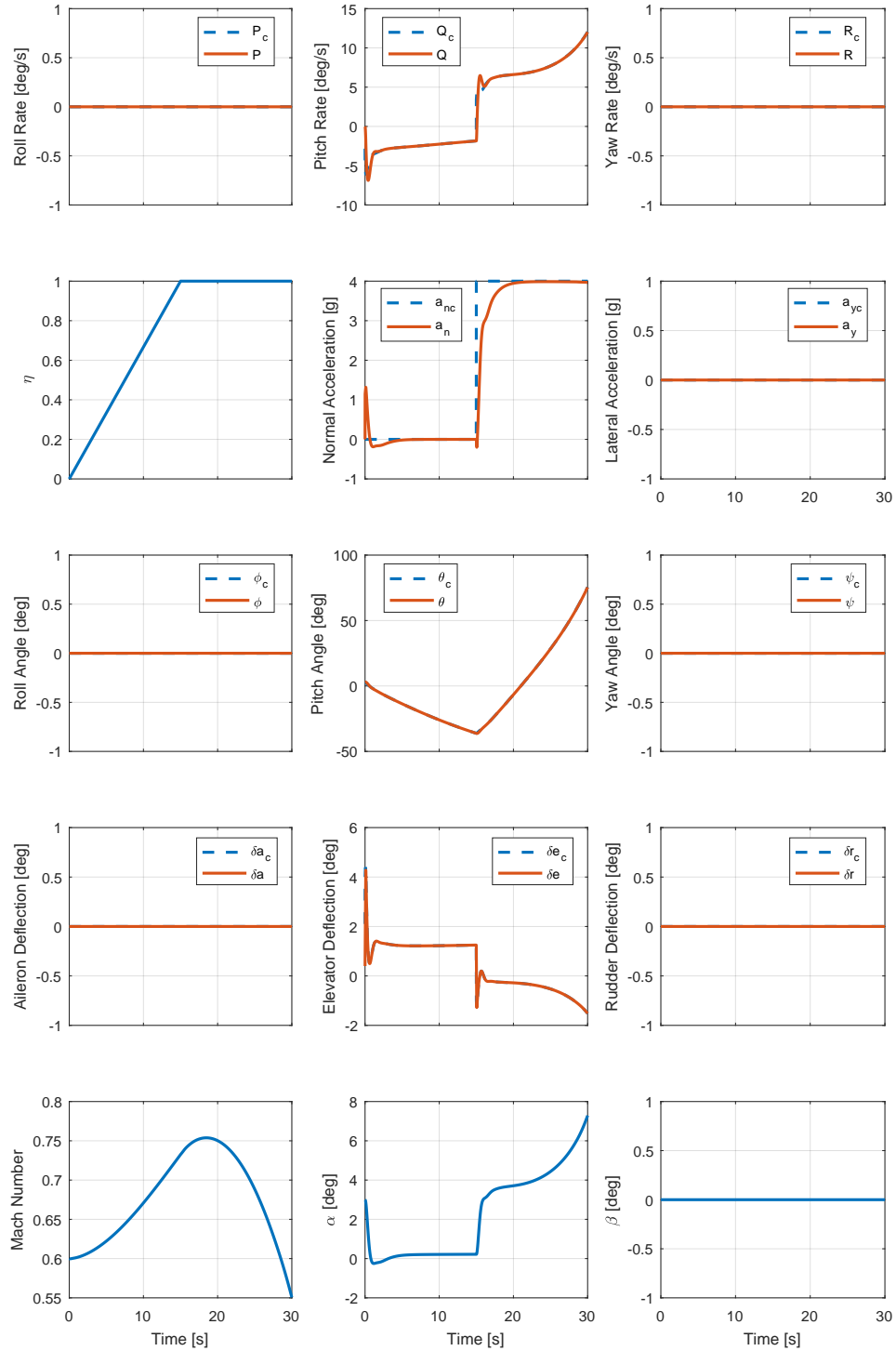


Figure 5: Push-over and pull-up (fixed throttle 0.4, exact inversion, altitude loss 792m)

NEURAL NETWORK-BASED NONLINEAR DYNAMIC INVERSION CONTROL OF VARIABLE-SPAN MORPHING AIRCRAFT

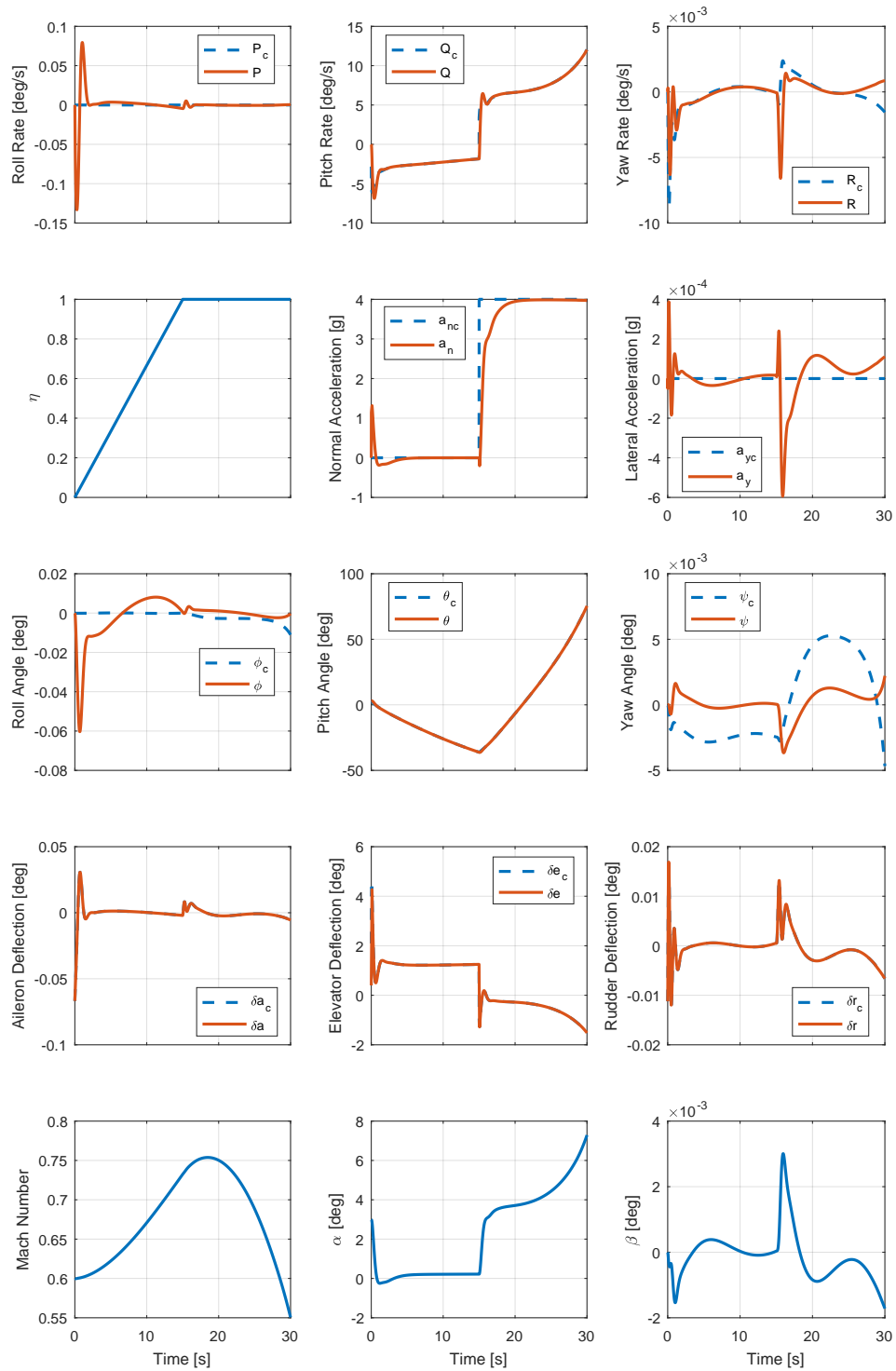


Figure 6: Push-over and pull-up (fixed throttle 0.4, neural network inversion, altitude loss 792m)

NEURAL NETWORK-BASED NONLINEAR DYNAMIC INVERSION CONTROL OF VARIABLE-SPAN MORPHING AIRCRAFT

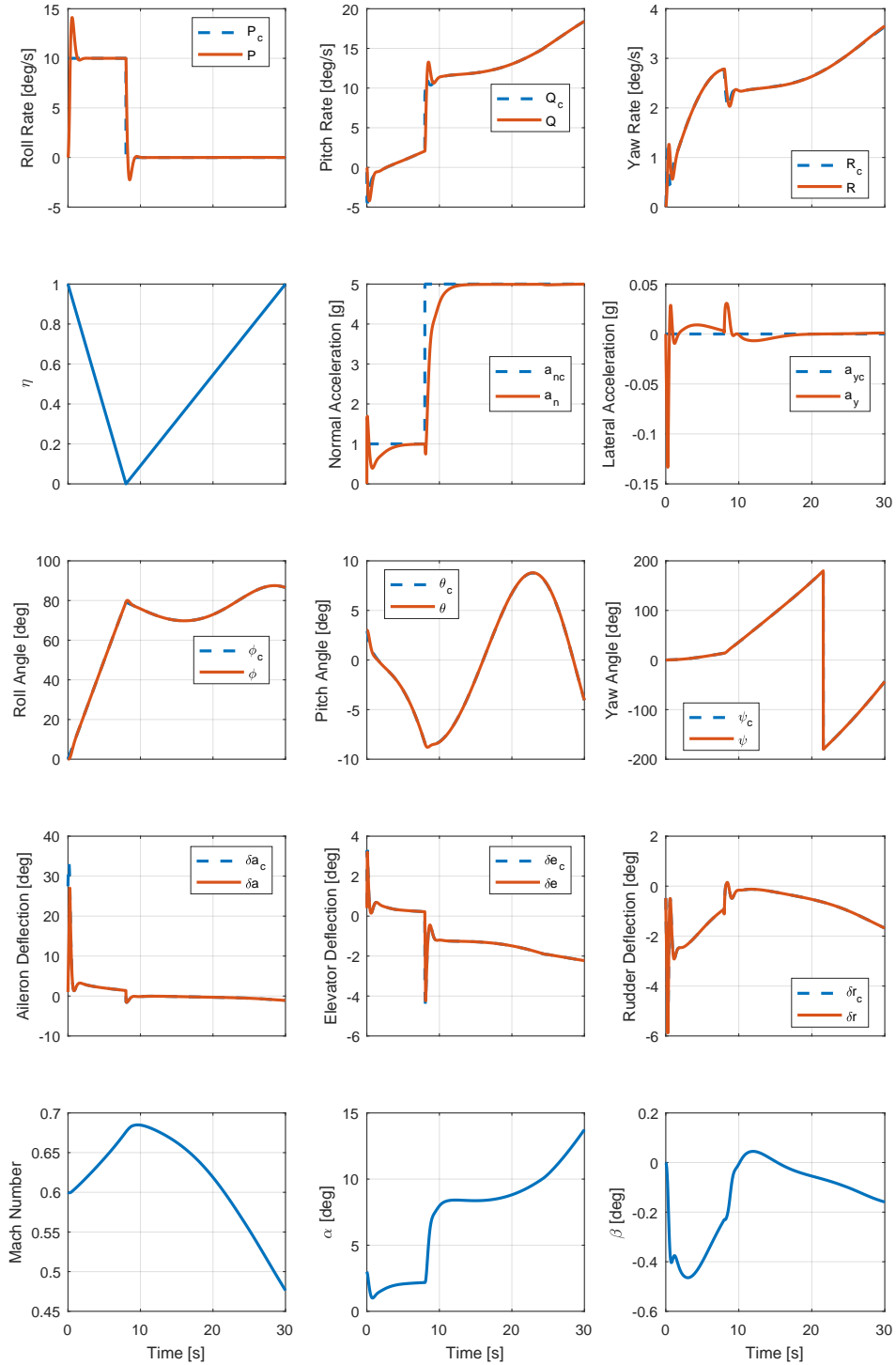


Figure 7: High-g turn (maximum throttle 1.0, exact inversion, altitude loss 212m)

NEURAL NETWORK-BASED NONLINEAR DYNAMIC INVERSION CONTROL OF VARIABLE-SPAN MORPHING AIRCRAFT

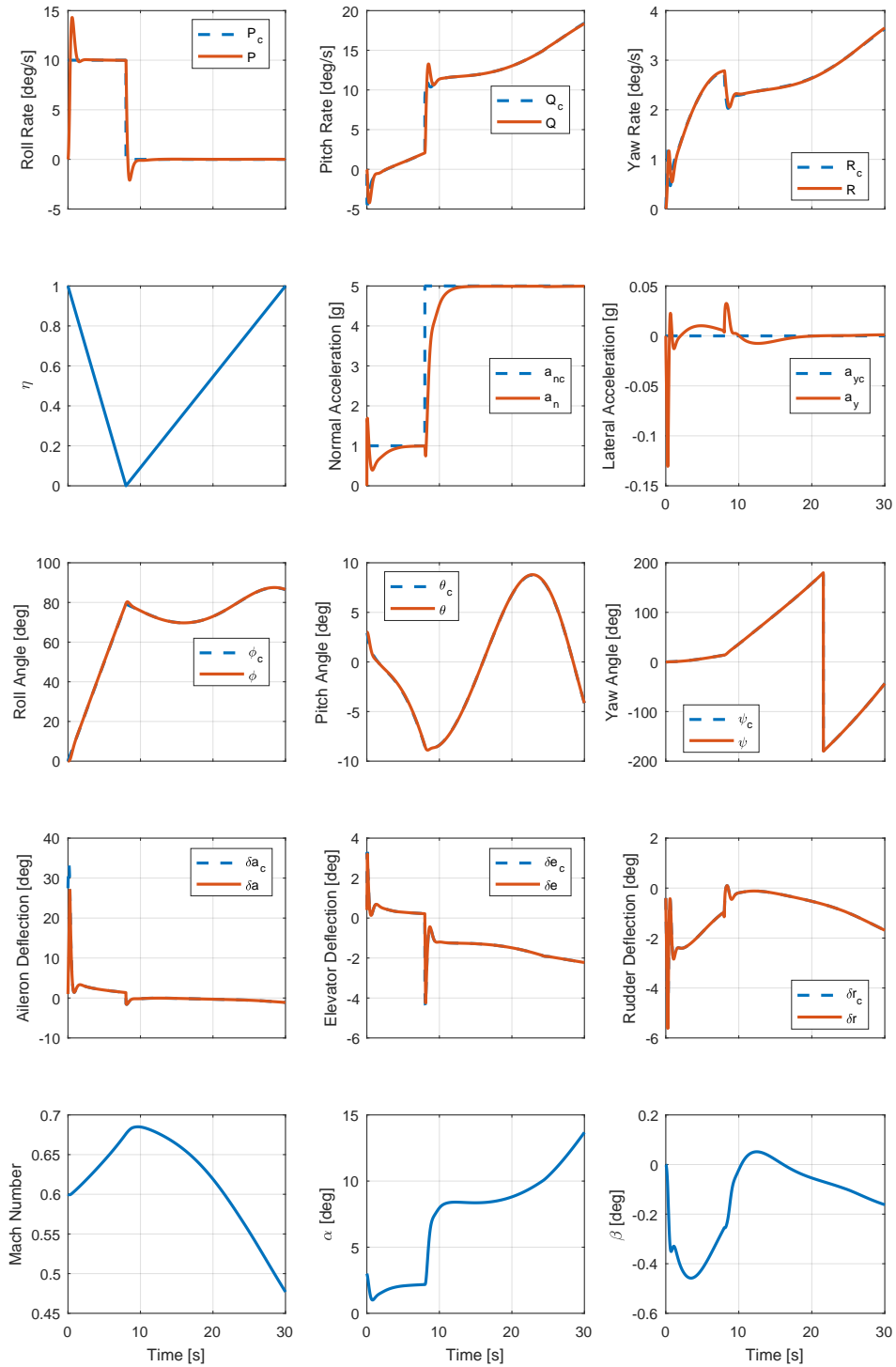


Figure 8: High-g turn (maximum throttle 1.0, neural network inversion, altitude loss 214m)

6. Conclusions

In this study, the structure of the command augmentation system (CAS) was generalized for adopting it to morphing aircraft. Two-layer neural networks for longitudinal and lateral channels were designed and trained to map desired aerodynamic moments into control surface deflection commands. The feed-forward neural network requires low computational load, which can be utilized in real-time operations. It can be inferred that neural network-based inversion can be applied to aircraft with arbitrary morphing configuration by simply adjusting the number of inputs in the neural network. Several combinations of backpropagation algorithms and hidden layer sizes were examined, and the best combination in terms of performance and overfitting was used for the CAS. Numerical simulation was performed for two maneuver scenarios to demonstrate the effectiveness of the proposed control scheme. A high-performance aircraft model was slightly modified to emulate the effect of span morphing. Simulation results showed that morphing aircraft can be effectively controlled by using the proposed control scheme.

7. Acknowledgments

This work was supported by the R&D Program in Aerospace Parts and Materials (10066055) through the Korea Evaluation Institute of Industrial Technology (KEIT) funded by the Ministry of Trade, Industry, and Energy (MOTIE), the Republic of Korea (ROK).

References

- [1] J. Valasek. *Morphing Aerospace Vehicles and Structures*. John Wiley & Sons, Chichester, United Kingdom, 2012.
- [2] C. Y. Dong, W. Li, and Q. Wang. H_∞ Control of Switched Systems with Nonideal Switchings and its Application to Morphing Aircraft. In *Procedia Engineering*, volume 67, pages 100–109, 2013.
- [3] T. Yue, L. Wang, and J. Ai. Gain Self-Scheduled H_∞ Control for Morphing Aircraft in the Wing Transition Process Based on an LPV Model. *Chinese Journal of Aeronautics*, 26(4):909–917, 2013.
- [4] W. Jiang, C. Dong, and Q. Wang. A Systematic Method of Smooth Switching LPV Controllers Design for a Morphing Aircraft. *Chinese Journal of Aeronautics*, 28(6):1640–1649, 2015.
- [5] J. Valasek, J. Doebbler, M. D. Tandale, and A. J. Meade. Improved Adaptive-Reinforcement Learning Control for Morphing Unmanned Air Vehicles. *IEEE Transactions on Systems, Man, and Cybernetics, Part B: Cybernetics*, 38(4):1014–1020, 2008.
- [6] J. Valasek, M. D. Tandale, and J. Rong. A Reinforcement Learning - Adaptive Control Architecture for Morphing. In *AIAA Intelligent Systems Technical Conference*, Chicago, IL, Sep. 2005.
- [7] J. Colorado, A. Barrientos, C. Rossi, and C. Parra. Inertial Attitude Control of a Bat-like Morphing-wing Micro Air Vehicle. *Bioinspiration & Biomimetics*, 8(1):1–25, 2013.
- [8] M. Bras, J. Vale, F. Lau, and A. Suleman. Flight Dynamics and Control of a Vertical Tailless Aircraft. *Journal of Aeronautics & Aerospace Engineering*, 2(4):1–10, 2013.
- [9] T. Wang, C. Dong, and Q. Wang. Finite-Time Boundedness Control of Morphing Aircraft Based on Switched Systems Approach. *Optik*, 126(23):4436–4445, 2015.
- [10] D. H. Baldelli, D Lee, R. S. S. Peña, and B. Cannon. Modeling and Control of an Aeroelastic Morphing Vehicle. *Journal of Guidance, Control, and Dynamics*, 31(6):1687–1699, 2008.
- [11] D. Li. Active Control Design for an Unmanned Air Vehicle with a Morphing wing. *Aircraft Engineering and Aerospace Technology: An International Journal*, 88(1):168–177, 2016.
- [12] T. M. Seigler, D. A. Neal, J. Bae, and D. J. Inman. Modeling and Flight Control of Large-Scale Morphing Aircraft. *Journal of Aircraft*, 44(4):1077–1087, 2007.
- [13] Z. He, M. Yin, and Y. Lu. Tensor Product Model-Based Control of Morphing Aircraft in Transition Process. *Proceedings of the Institution of Mechanical Engineers, Part G: Journal of Aerospace Engineering*, 230(2):378–391, 2016.

NEURAL NETWORK-BASED NONLINEAR DYNAMIC INVERSION CONTROL OF VARIABLE-SPAN MORPHING AIRCRAFT

- [14] T. M. Seigler and D. A. Neal. Analysis of Transition Stability for Morphing Aircraft. *Journal of Guidance, Control, and Dynamics*, 32(6):1947–1954, 2009.
- [15] R. Pecora, F. Amoroso, and L. Lecce. Effectiveness of Wing Twist Morphing in Roll Control. *Journal of Aircraft*, 49(6):1666–1674, 2012.
- [16] P. Bourdin, A. Gatto, and M. I. Friswell. Aircraft Control via Variable Cant-Angle Winglets. *Journal of Aircraft*, 45(2):414–423, 2008.
- [17] L. Tong and H. Ji. Multi-Body Dynamic Modelling and Flight Control for an Asymmetric Variable Sweep Morphing UAV. *Aeronautical Journal*, 118(1204):683–706, 2014.
- [18] T. Yue, L. Wang, and J. Ai. Longitudinal Linear Parameter Varying Modeling and Simulation of Morphing Aircraft. *Journal of Aircraft*, 50(6):1673–1681, 2013.
- [19] A. Chakravarthy, D. T. Grant, and R. Lind. Time-Varying Dynamics of a Micro Air Vehicle with Variable-Sweep Morphing. *Journal of Guidance, Control, and Dynamics*, 35(3):890–903, 2012.
- [20] B. Obradovic and K. Subbarao. Modeling of Dynamic Loading of Morphing-Wing Aircraft. *Journal of Aircraft*, 48(2):424–435, 2011.
- [21] B. Obradovic and K. Subbarao. Modeling and Simulation of Morphing Wing Aircraft. *Journal of Aircraft*, 48(2):87–125, 2012.
- [22] Y. Shin, M. D. Johnson, and A. J. Calise. Neural Network-Based Adaptive Control for Nonlinear Flight Regimes. In *AIAA Guidance, Navigation, and Control Conference*, Austin, TX, Aug. 2003.
- [23] T. Lee and Y. Kim. Nonlinear Adaptive Flight Control Using Backstepping and Neural Networks Controller. *Journal of Guidance, Control, and Dynamics*, 24(4):675–682, 2001.
- [24] S. Suresh, S. N. Omkar, V. Mani, and N. Sundararajan. Direct Adaptive Neural Flight Controller for F-8 Fighter Aircraft. *Journal of Guidance, Control, and Dynamics*, 29(2):454–464, Mar. 2006.
- [25] D. Sadhukhan and S. Feteih. F8 Neurocontroller Based on Dynamic Inversion. *Journal of Guidance, Control, and Dynamics*, 19(1):150–156, 1996.
- [26] J. O. Pedro and N. D. Meyer. Neural Network-Based Dynamic Inversion Controller for Fighter Aircrafts. In *IFAC Symposium on Nonlinear Control Systems*, Pretoria, Aug. 2007.
- [27] C. Schuhmacher and J. D. Johnson. PI Control of a Tailless Fighter Aircraft with Dynamic Inversion and Neural Networks. In *American Control Conference*, San Diego, CA, Jun. 1999.
- [28] W. Gai, H. Wang, J. Zhang, and Y. Li. Adaptive Neural Network Dynamic Inversion with Prescribed Performance for Aircraft Flight Control. *Journal of Applied Mathematics*, (Article ID 452653):1–12, 2013.
- [29] Lili and H. Zhang. Neural Network Based Adaptive Dynamic Inversion Flight Control System Design. In *International Conference on Intelligent Control and Information Processing*, Harbin, China, Jul. 2011.
- [30] P. K. A. Menon. Nonlinear Command Augmentation System for a High Performance Aircraft. In *AIAA Guidance, Navigation, and Control Conference*, Monterey, CA, Aug. 1993.
- [31] B. S. Kim. Nonlinear Flight Control Using Neural Networks, Ph.D. Dissertation, Department of Aerospace Engineering, Georgia Institute of Technology, Atlanta, GA, 1993.
- [32] B. S. Kim and A. J. Calise. Nonlinear Flight Control Using Neural Networks. *Journal of Guidance, Control, and Dynamics*, 20(1):26–33, 1997.